2018

Improved Equivalent Simple Model of Complicated Bypass Leakages in Scroll Compressors

Keiko Anami
Osaka Electro-Communication University, anami@osakac.ac.jp

Noriaki Ishii
Osaka Electro Communication University, ishii@isc.osakac.ac.jp

Takuma Tsuji
Mayekawa MFG. Co., Ltd., takuma-tsuji@mayekawa.co.jp

Charles W. Knisely
Bucknell University, knisely@bucknell.edu

Improved Equivalent Simple Model of Complicated Bypass Leakages in Scroll Compressors

Keiko ANAMI[1*], Noriaki ISHII[1], Takuma TSUJI[2],& Charles W. KNISELY[3]

[1] Osaka Electro-Communication University, Department of Mechanical Engineering
Neyagawa, Osaka, Japan.
anami@osakac.ac.jp, ishii@isc.osakac.ac.jp

[2] Mayekawa Mfg. Co., Ltd., Research and Development Center
Moriya, Ibaraki, Japan
takuma-tsuji@mayekawa.co.jp

[3] Bucknell University, Mechanical Engineering Department
Lewisburg, PA, USA
knisely@bucknell.edu

ABSTRACT

This study presents an improved simple equivalent model to calculate the bypass leakage mass flow rate along the tip seal in scroll compressors, where the complicated flow patterns through bypass clearances were decomposed into two thin representative rectangular cross-section leakage passes. The one is for the leakage along the tip seal and has the rectangular cross-section of the effective mean width by the thrust clearance height over the scroll wrap in front of the tip seal, where the pass length was represented by the equivalent leakage length, theoretically derived from the simple Darcy-Weisbach equation. The other is for the tangential leakage over the scroll wrap, through the minimum rectangular cross-section in front of the tip seal, and the pass length was represented by the effective mean length. The effective mean width and length were empirically determined with simple bypass leakage tests, where the pressure decay in a pressurized vessel with dry refrigerant gas R410A, due to the bypass leakages, were measured. The measured pressure decay characteristics were subsequently simulated using the Darcy-Weisbach equation with an empirical friction factor determined in our previous study for the leakage flow through axial clearances. Empirical values of the effective pass width and length were determined so that the measured pressure decays are well predicted by the calculations. Furthermore the effective pass width and length were reduced to a non-dimensional form and the physical meanings represented by the empirical values were examined, and finally the leakage flow velocities and leakage flow rates were presented.

1. INTRODUCTION

A previously developed simple equivalent method to calculate the bypass leakage mass flow rate along the tip seal in scroll compressors assumed that the pressure loss due to the tangential flow through the slot under the tip seal is negligible, as its cross-sectional area is comparatively large (see Ishii *et. al.*, 2016). However, our subsequent studies showed that the assumption was wrong. Therefore, the present study was carefully carried out to develop an improved simple equivalent model to calculate the complicated bypass leakages, explicitly accounting for the previously ignored pressure loss.

Our study proposes that the complicated flow patterns through bypass clearances can be classified into two representative flows through thin rectangular cross-sectional passages. One is for the leakage flow from the radial flow over the scroll wrap, to the axial flow in front of the tip seal, to the tangential flow through the tip seal slot, and then to the axial and radial flows, and which is denoted as leakage flow *Model-1*; it has a rectangular cross-section given by the product of the effective mean passage width and the thrust clearance height above the scroll wrap in front of the tip seal with a passage length represented by the equivalent leakage length which is theoretically derived using the Darcy-Weisbach equation with the momentum equation for incompressible viscous fluid under fully-developed

turbulent flow. The other – for tangential leakage over the scroll wrap, through the narrowing and spreading cross-section in front of the tip seal– is denoted as leakage flow *Model-2*, in which the passage length is represented by the effective mean passage length to account for tangential leakage.

In the present study the leakage passage effective mean width and effective mean length are determined from very simple bypass leakage tests, where the pressure drop characteristics due to leakages are measured in detail. For this purpose, a bypass leakage laboratory test model with precise clearances is developed to emulate a scroll compressor with a large cooling capacity. The resulting pressure drop in an attached large vessel with dry refrigerant gas R410A, pressurized up to 1.1 MPa, are measured. Initially, in the present tests, the flow passage of *Model-1* was completely sealed and the pressure drop only due to the leakage through the flow passage of *Model-2* was measured to identify the effective mean passage length for *Model-2* by forcing the theoretically calculated results to agree well with the pressure drop slope just at the start of the measurements. Subsequently, similar tests and theoretical calculations were conducted for the combined leakage flow *Model-1&2* after entirely removing the *Model-1* seals, permitting the identification of the effective mean passage width for *Model-1*. Next, the pressure drop characteristics were theoretically calculated over the range of measurements, using the identified effective mean width and effective mean length of leakage passages, and showed good agreement with the test results. Additionally, the leakage passage effective mean width and effective mean length were reduced to non-dimensional forms, permitting the assessment of the physical meaning represented by the empirical values. Finally, the leakage flow velocities and leakage mass flow rate were computed and examined. The utility of applying of this method to other scroll compressor geometries is suggested for future studies.

2. EQUIVALENT LEAKAGE FLOW MODEL WITH PARALLEL PASSAGES WITH RECTANGULAR CROSS-SECTION

2.1 Basic Configuration of Bypass Leakage Flows

The configuration of general installation of the tip seals into a rectangular slot machined on the top of the scroll wrap is shown in Figure 1(a). The right hand side faces a high pressure region and the left hand side faces a low pressure region. The tip seals are pressed against the left side wall of the slot and upward onto the orbiting thrust plate, caused by hydrodynamic effects. Nonetheless, leakage clearances δ_{r0} and δ_{a0} remain behind and above the tip seal, respectively. In the present study, however, these leakages through these clearances δ_{r0} and δ_{a0} (labelled ①', ②', ⑤', ④'), are assumed to be negligible when compared with the other leakages. The major bypass leakages occur through

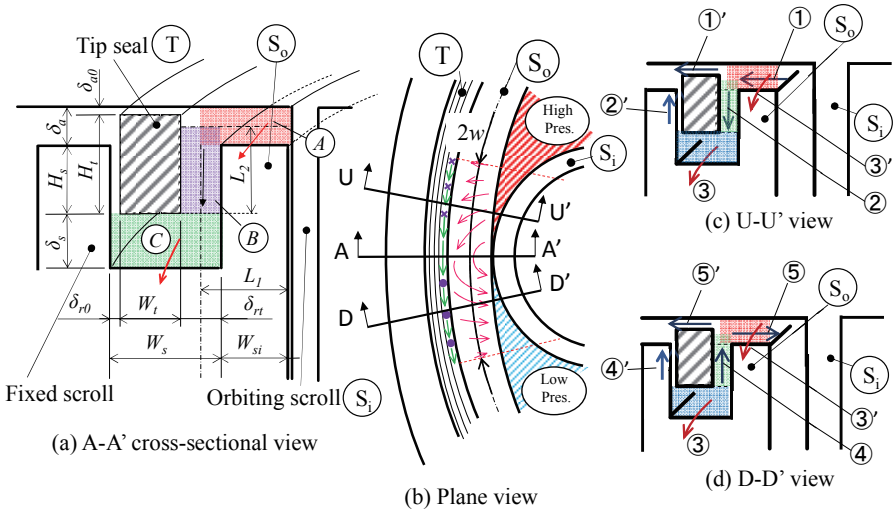

Figure 1: Configuration of bypass leakage flows:
(a) A-A' cross-sectional view of installation of tip seal into slot on scroll wrap; (b) Top view of bypass leakage flow patterns; (c) U-U' cross-sectional view of in-flow from high pressure region to tip-seal slot; (d) D-D' cross-sectional view of out-flow from tip-seal slot to low pressure region

the leakage region "A" over the front scroll wrap, the leakage region "B" in front of the tip seal and the leakage region "C" in the tip seal slot. A top view of the bypass leakage flow patterns is illustrated in Figure 1(b). The flow in the region "A" above the scroll wrap consists of radial and tangential flows. The radial flow (labelled ①) from the high pressure region changes its direction downward in front of the tip seal and flows into the region "B" (labelled ②) and then into the slot under the tip seal; furthermore, the flow changes its direction again in the tangential direction along the tip seal slot indicated in region "C" (labelled ③), as shown in Figure 1(c). The out-flow (labelled ③ to ⑤) from the tip seal slot into the low pressure region mirrors the in-flow (labelled ① to ③), as explained above, and shown in Figure 1(d). The tangential flow in the region "A" (labelled ③') directly flows from the high pressure region into the low pressure region.

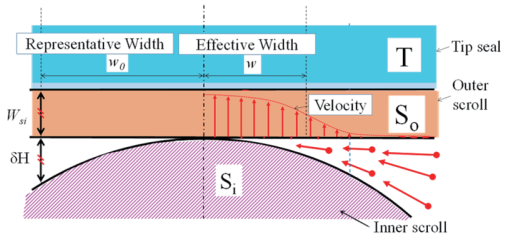

Figure 2: Effective mean passage width for radial flow over outer scroll (scroll wrap, labelled S_o) and its representative value for non-dimensional form

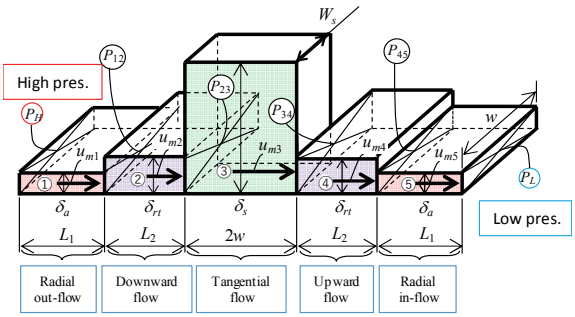

Figure 3: Equivalent step-like passages with effective width, for flows labelled 1 to 5 of bypass leakage

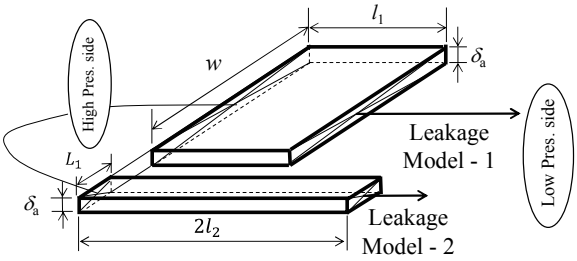

Figure 4: Equivalent flow model of parallel rectangular-cross-section passage, consisted of *Model 1* and *Model 2*, for bypass leakages

2.2 Equivalent Parallel Rectangular-Cross-Section Passages

The in- and out-flows, labelled ① to ⑤, are classified as a leakage flow *Model-1*, which can be represented as the leakage flow through a simple thin rectangular cross-sectional passage with the effective mean passage width and an equivalent length. The fundamental idea for the effective mean passage width is developed in Figure 2. The radial in-flow velocity distribution along the tangential direction over the scroll wrap is illustrated. The high pressure region between the outer scroll S_o and the inner scroll S_i forms a wedge, and hence the refrigerant gas is concentrated into the tip of the wedge and then flows out in the radial direction over the outer scroll, thus exhibiting an increase in radial flow velocity as it approaches the contact point of the outer and inner scrolls. This kind of flow may be analyzed with FEM computer calculations, but such a time-consuming method is seldom effective in practical calculations of the volumetric efficiency of scroll compressors under a variety of various operating conditions. A very simple scheme to roughly evaluate this leakage flow, which in turn can afford an accurate calculation of the leakage mass flow rate, is essential. For this purpose, the concept of "effective mean width", represented by w, is introduced, in which the flow velocity is assumed constant. The proposed effective mean passage width depends naturally upon the pressure difference between the high and low pressure regions; its empirical value can be easily determined by leakage tests.

With the introduction of the effective mean passage width w, the in- and out-flows, labelled ① to ⑤, can be represented by a very simple step-like passage with the same effective mean passage width for all the flow steps, as shown in Figure 3. However, the flow passage width for the tip seal slot flow, labelled ③, results in W_s. The clearance and length of each passage is δ_a and L_1 for the flows ① and ⑤, while δ_s and $2w$ for the flow ③, δ_{rt} and L_2 for the flows ② and ④. L_1 and L_2 are given by the values added each actual pass length to 1/2 of δ_{rt} and δ_a, respectively.

Here, the Darcy-Weisbach equation is applied to each flow labelled ①, ②, ③, ④ and ⑤:

$$\frac{P_H - P_{12}}{\rho g} = \lambda \frac{L_1}{2\delta_a} \frac{u_{m1}{}^2}{2g}, \quad \frac{P_{12} - P_{23}}{\rho g} = \lambda \frac{L_2}{2\delta_{rt}} \cdot \frac{u_{m2}{}^2}{2g}, \quad \frac{P_{23} - P_{34}}{\rho g} = \lambda \frac{2w}{2\delta_s} \left(\frac{\delta_s}{W_s} + 1\right) \cdot \frac{u_{m3}{}^2}{2g},$$
$$\frac{P_{34} - P_{45}}{\rho g} = \lambda \frac{L_2}{2\delta_{rt}} \frac{u_{m4}{}^2}{2g}, \quad \frac{P_{45} - P_L}{\rho g} = \lambda \frac{L_1}{2\delta_a} \frac{u_{m5}{}^2}{2g} \tag{1}$$

In the previous study (Ishii *et al.*, 2016), the pressure loss for the flow labelled ③ was disregarded since the passage cross-section area is comparatively large and the corresponding pressure loss due to flow friction was assumed to be negligible. Our later studies, however, showed that the pressure loss cannot be disregarded; thus, the pressure loss through flow passage ③ is included in the present more precise analysis. P represents the pressure and u_m the flow velocity. The density ρ is constant (incompressible flow assumption) and g is gravitational acceleration. The hydraulic diameter is given by $2\delta_a$ for the flow passages ① and ⑤, and $2\delta_{rt}$ for the flow passages ② and ④. In contrast, the hydraulic diameter for the flow passage ③ is given by 4 times $\delta_s W_s/\{2(\delta_s + W_s)$ which is the hydraulic mean depth of the rectangular cross-section with the flow passage width W_s and clearance height δ_s. Pressure losses due to flow bending and large area expansion and contraction have been neglected. The continuity equations require that

$$u_{m1}\delta_a w = u_{m2}\delta_{rt} w = u_{m3}\delta_s W_s = u_{m4}\delta_{rt} w = u_{m5}\delta_a w\,. \tag{2}$$

The summation of each side of the Darcy-Weisbach equations in (1), with consideration of the continuity equation (2), results in the following:

$$\frac{P_H - P_L}{\rho g} = \lambda \frac{l_1}{2\delta_a} \frac{u_{m1}^2}{2g}, \text{ where } l_1 \equiv 2L_1 + 2L_2 \left(\frac{\delta_a}{\delta_{rt}}\right)^3 + W_s \left(\frac{\delta_a}{\delta_s} \cdot \frac{2w}{W_s}\right)^3 \left(\frac{\delta_s}{W_s} + 1\right) \tag{3}$$

Equation (3) represents the reduction of the step-like passages, shown in Figure 3, to the simplest rectangular cross-section passage, as shown by the leakage *Model-1* in Figure 4. The clearance height is δ_a. The equivalent length l_1 is defined in Equation (3).

An additional leakage, beyond that of *Model-1*, is the tangential upstream and downstream flows over the scroll wrap, labelled ③', as shown in Figures 1(c) and (d). This tangential flow through the minimal rectangular cross-section with the clearance height δ_a and the width L_1 can be simply represented by a flow through the rectangular cross-section passage with the effective mean passage length $2l_2$, as shown by the leakage *Model-2* in Figure 4. The leakage flow through *Model-2* is also modeled using the Darcy-Weisbach equation:

$$\frac{P_H - P_L}{\rho g} = \lambda \frac{2l_2}{2\delta_a} \frac{u_m^2}{2g}\,. \tag{4}$$

The leakage-induced pressure drop tests were initially conducted to determine the empirical value of the effective mean passage length l_2 for the leakage passage *Model-2*. Subsequently, the leakage-induced pressure drop tests were repeated for the combined leakage passage *Model-1&2* to determine the effective mean passage width w.

3. EMPIRICAL VALUES OF EFFECTIVE MEAN LENGTH AND WIDTH OF PARALLEL RECTANGULAR CROSS-SECTION PASSAGES

3.1 Leakage Test Set-Up

Photos of the present leakage test set-up are shown in Figure 5. The mating scrolls are both curved, and the scroll on the tip seal side, S_0, is made straight, for easy high-precision machining, while the mating scroll S_i is curved with a radius of 241 mm. Such a model represents the form which tapers toward the scroll contact point. The plane drawing

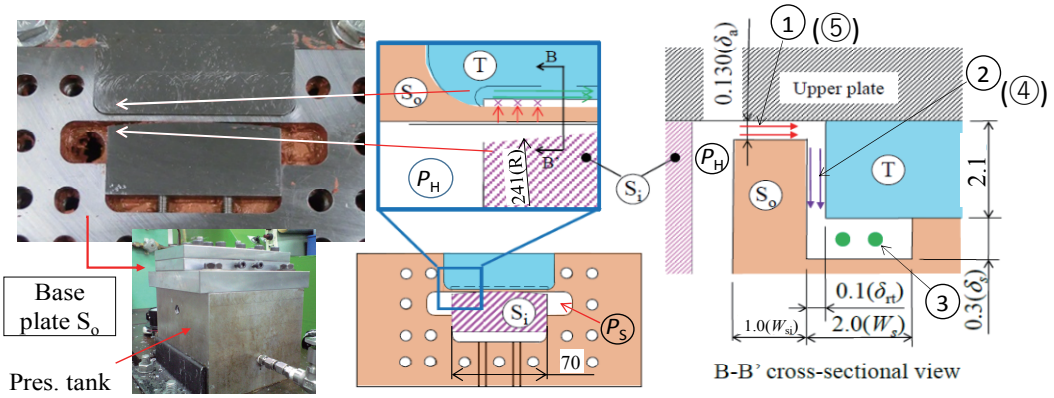

Figure 5: Configuration of lubrication test set-up.

is shown in the center of Figure 5, and the B-B' section view is on the right side. The straight tip seal slot with a width W_s of 2.0 mm and a depth of 2.4 mm is machined on the straight scroll S_0 at 1.0 mm (W_{si}) from its front face. The outer face of the slot is machined down 0.13 mm to secure the axial clearance height δ_a, while the inner is machined down 2.1 mm. The straight tip seal T with a thickness of 2.1 mm is mounted on the inner face, and thus the upper face of T is on the same level as the original upper face of S_0 and the slot with a depth of 0.3 mm (δ_s) is left under T. The front face of T is machined by 0.1 mm to secure precisely the radial clearance δ_{rt}. The leakage flow passages ① to ⑤ labeled in Figure 1(c) and 1(d) can be precisely modeled with the present set-up. The major specifications for the present leakage tests are listed in Table 1. The pass length L_1 for leakage flows ① & ⑤ and L_2 for leakage flows ② & ④ are 1.06 mm and 2.035 mm, respectively.

The test model is sandwiched between the upper and lower plates and fixed on the lower-side pressurized tank, as shown in photos on the left side of Figure 5. In the process of fixing, careful attention was paid to seal perfectly the contact surfaces between the parts, with a fluid gasket, so that the bypass passages are not sealed. The high pressure chamber of P_H is connected to the pressurized tank with a volume of 860 cm^3. The low pressure region of P_S is connected to a refrigerant recovery tank through the release valve.

Table 1: Major specifications for bypass leakage tests.

Pass length L_1 [mm]	1.05
Pass length L_2 [mm]	2.035
High pressure P_H [MPa]	0.4～1.2
Low pressure P_S [MPa]	0.1
Inner scroll radius R [mm]	241
Slot width W_s [mm]	2.0
Width W_{st} [mm]	1.0
Axial clearance δ_a [μm]	130
Radial clearance δ_{rt} [μm]	100
Slot height δ_s [μm]	300

Table 2: Initial conditions of temperature, density ρ_0 and viscous coefficient μ for leakage tests with pressure difference ΔP up to 1.1 MPa.

	Model－1&2			Model－2		
ΔP (MPa)	Temp. (K)	Density ρ_0 (kg/m^3)	μ (×10^{-6} Pa･s)	Temp. (K)	Density ρ_0 (kg/m^3)	μ (×10^{-6} Pa･s)
1.1	295.05	43.65	13.34	295.65	43.46	13.37
1.0	294.15	39.36	13.27	295.65	38.97	13.34
0.9	293.25	35.22	13.21	295.75	34.68	13.32
0.8	293.45	31.01	13.20	295.65	30.62	13.30
0.7	294.35	26.90	13.22	295.75	26.71	13.29
0.6	293.95	23.16	13.19	296.25	22.90	13.29
0.5	294.85	19.43	13.22	296.45	19.29	13.29
0.4	295.05	15.91	13.22	296.65	15.80	13.29
0.3	294.85	12.54	13.21	296.75	12.44	13.29
0.2	294.75	9.27	13.20	297.25	9.18	13.31
0.1	294.55	6.09	13.19	297.05	6.04	13.30

3.2 Pressure Decay Test Results and Determination of Effective Mean Width for Leakage Model-1 and Effective Mean Length for Leakage Model-2

The test itself is very simple and easily conducted. Initially, the release valve is closed to extract air with a vacuum pump from inside of the whole system. Then the system is charged with refrigerant gas R410A. The release valve is opened as quickly as possible and the pressure decay in the pressurized tank, due to gas leakage, is measured until the pressure in the high pressure tank decreases to atmospheric pressure. The initial high pressure in the tank, $P_{H,}$ was

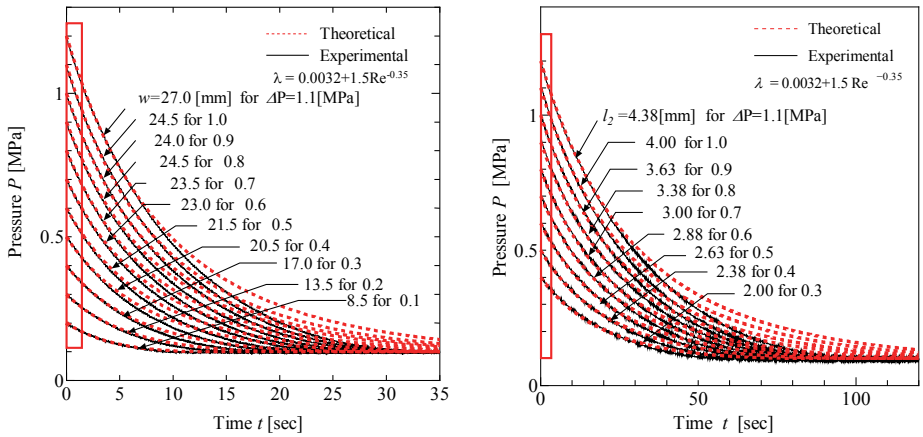

(a) Pressure decay for Model-1&2. (b) Pressure decay for Model-2.

Figure 6: Measured time-dependent pressure decay characteristics and theoretical simulation for determining effective mean passage width *w* for *Model-1* and effective mean passage length l_2 for *Model-2*.

increased from 0.2 MPa to 1.2 MPa in steps of 0.1 MPa, relative to the atmospheric low pressure P_S of 0.1 MPa. Thus, the pressure difference Δp changed from 0.3 to 1.1 MPa. The initial conditions for the present leakage tests are presented in Table 2.

The pressure decay due to bypass leakage was detected with a pressure transducer (JTEKT, PMS-5M). Measured pressure characteristics are shown by a solid line (black) in Figure 6. Figure 6(a) shows the transient pressure decay due to the resultant leakage for combined *Models-1&2*, while Figure 6(b) shows the pressure decay due to a leakage only for *Model-2*, where the leakage passages for *Model-1* were completely and carefully sealed. The leakage cross-section area for *Model-2* is v ery small compared with that for *Model-1* and, hence, the pressure decay shown in Figure 6(b) takes far more time the pressure decay shown in Figure 6(a) for *Models-1&2*.

The empirical friction factor λ in the Darcy-Weisbach equation was empirically determined by Ishii et al. (1996, 2011) and Oku et al. (2005), which together indicated that λ–values are essentially independent of the kind of refrigerant. Furthermore, our recent studies revealed in detail the effects of temperature, surface roughness and oil wetness. As a result, the empirical friction factor λ can be represented by a Nikuradse-style turbulent flow formula:

$$\lambda = 0.0032 + 1.5\,\mathrm{Re}^{-0.35}, \text{ where the Reynolds number is } \mathrm{Re} \equiv 2\delta_a \rho u_m / \mu, \tag{5}$$

This empirical formula, considered most reliable at the present stage, was used for the present theoretical calculations of pressure drop (the details of research will be reported in near future). The viscosity is given byμ; the Reynolds number is *Re* reaching a maximum value of 1.4×10^5 in the present tests. The empirical friction factor λ in over a range of Reynolds number is shown by the solid line on the Moody diagram (for pipe flows) in Figure 7. The mean roughness of the leakage flow passages of the present test model, ε, was 0.34 μm, and the clearance height δ was 130 μm for the flow pass ① and 100 μm for the flow pass ②. As a result, the relative roughness $\varepsilon/d(=\varepsilon/2\delta)$ for the equivalent circular pipe takes about 0.002. The leakage flow velocity u_{m1} and u_m can calculated from be Equations (3) to (5), and thus the mass flow rate $\dot{m}$ can be calculated by

$$\dot{m} = \rho\delta_a w u_{m1} \text{ for Model-1 or } \rho\delta_a W_{si} u_m \text{ for Model-2} \tag{6}$$

where the density ρ can be calculated by

$$\rho = \rho_0 \left(P / P_0\right)^{1/n}. \tag{7}$$

The initial pressure and density are represented by P_0 and ρ_0, respectively. The residual refrigerant mass in the high pressure chamber, G, can be calculated by subtracting the total leakage mass from the initial refrigerant mass G_0:

$$G = G_0 - \int_0^t \dot{m} dt \tag{8}$$

G_0 can be calculated with the initial density and the pressurized tank volume (860 cm^3). Finally, assuming a polytropic process with exponent n, the pressure decay ΔP in the high pressure chamber over a small time Δt can be calculated:

$$\Delta P = \frac{P_0}{G_0^n} n G^{n-1} \dot{m} \Delta t. \tag{9}$$

Given the initial temperature and pressure, the initial density ρ_0 and viscosity coefficient μ for R410A are determined from the refrigerant characteristics program (REFPROP 8.0 NIST, 2007), as listed in Table 2. Next, the leakage flow velocity can be calc ulated using Equation (3) or (4) and Equation (5) representing the empirical friction factor λ and the Reynolds number Re, with the repeated calculation method. Subsequently, the mass flow rate can be calculated from Equations (6) and (7), and the refrigerant mass which remained in the pressurized tank from Equation (8) and finally the pressure drop value from Equation (9).

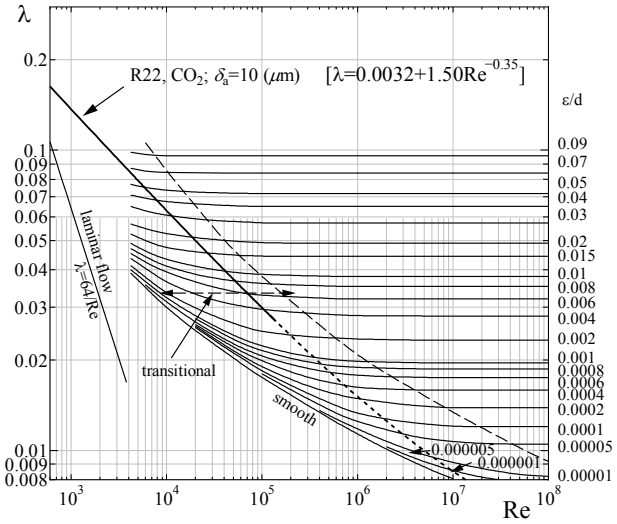

Figure 7: Empirical friction factor on the Moody diagram.

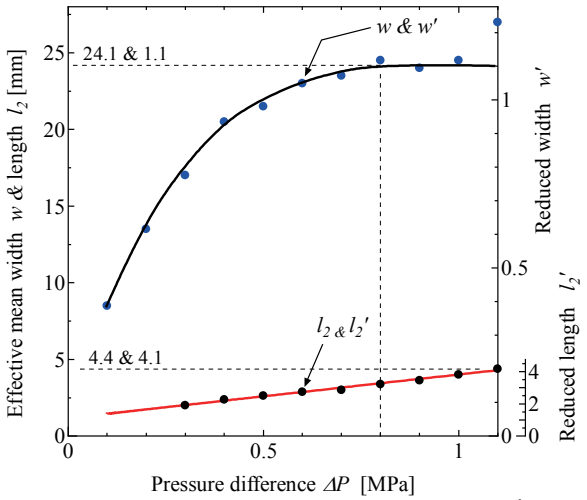

Figure 8: Effective mean passage widths w and w' as well as lengths l_2 and l_2', determined from pressure decay tests

First in theoretical simulation of the pressure drop curve, the effective mean passage length l_2 was identified by repeated assumption of an empirical value which when fitted to test results for *Model-2*, shown in Figure 6(b), gave a computed transient pressure that matched the measured pressure drop curve (solid line), over the short time range (marked by the slender aspect ratio rectangle) just after starting measurement. Using the converged value of passage length l_2 in the pressure drop calculation yielded the predicted curve with a negative slope (dashed line). Similar simulations were conducted for each set of the measured pressure drop data, thus identifying the effective mean passage length l_2 for each initial pressure difference ΔP, as denoted as the parameter. In addition, the empirical values are shown over the initial pressure difference ΔP in Figure 8. Then, using the identified empirical values for l_2, the pressure drop for combined *Model-1&2*, shown in Figure 6(a), was theoretically calculated for an assumed value of w. As in the *Model-1* case, the effective mean passage width w was iterated until the measured pressure drop curve over a small time range just after starting measurement was well predicted by the theoretical calculations. The empirical values of w are included as the parameter in Figure 6(a) and in Figure 8. With increasing pressure difference ΔP, the effective mean passage length l_2 increases linearly to about 4.4 mm at ΔP =1.1 MPa. The effective mean passage width w exhibits a monotonic, non-linear increase and approaches about 24.1 mm at ΔP =1.1 MPa. These results suggest that the leakage flow is enhanced with decreasing pressure.

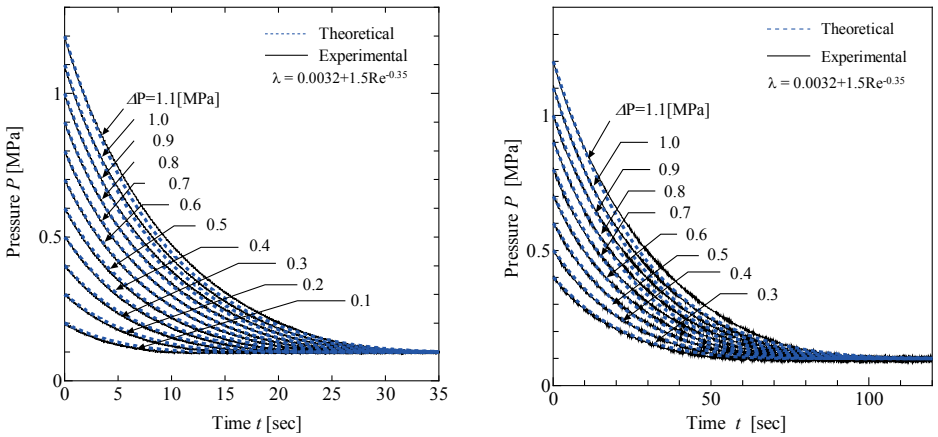

(a) *Model-1&2* (b) *Model-2*

Figure 9: Theoretical simulation of pressure decay for *Model-1&2* and *Model-2* compared with measured data

4. CONFIRMATION OF VALIDITY OF EMPIRICAL CALCULATION METHOD

As shown in Figu re 6, the theoretically simulated values of pressure decay diverge from the measured values with larger values of time. This difference is due assuming constant values of the effective mean passage width w and passage length l_2 in the simulations. The values for these two parameters were kept at the values determined from the data at the time immediately after the measurement started. In fact, however, both w and l_2 decreases as the pressure decreases, as shown in Figure 8, suggesting that leakage flow increases with decreasing the pressure. Therefore, if the pressure-dependent empirical values of w and l_2 , shown in Figure 8, are included in the theoretical simulations, the simulated the pressure decay is expected come into close agreement over the entire time duration. Such simulated pressure decay characteristics, including the empirical pressure-dependent parameters, as shown in Figures 9(a) and 9(b), confirm this expectation. In Figures 9(a) and 9(b), the calculated results are shown by the blue dashed lines agree well agreement with the measured values (solid black lines) over the entire duration. As a result, one may conclude that by including the tendency for increased leakage with decreasing pressure, the proposed very simplified method of representing the complicated bypass leakage flows by the flows through parallel rectangular cross-section passages can reproduce measured data with high accuracy.

Furthermore, the effective mean passage width w can be normalized by the representative tangential length w_0, presented in Figure 2, and the effective mean passage length l_2 by the width L_1 of the passage cross-section "A" labelled in Figure 1(a):

$$w' \equiv \frac{w}{w_0}, \quad \ell_2{}' \equiv \frac{l_2}{L_1} \tag{10}$$

in which w_0 is the horizontal (tangential) length from the contact point to the position where the clearance height δH between the outer and inner scrolls becomes equal to the scroll thickness in front of the tip seal, W_{si} (see Figure 2), taking on a value of 22.0 mm for the present test set-up.

The values of normalized quantities, denoted as the reduced mean passage width w' and the reduced mean passage length l_2' are plotted on secondary axis to the right in Figure 8. The reduced mean width $w'(\equiv w / w_0)$ exhibits a monotonic increase approaching the asymptotic value of about 1.1 for values of ΔP larger than 0.8 MPa. It is suggested that the reduced mean width w' is appropriate for most standard scroll designs. On the other hand, the reduced mean passage length l_2' increases linearly to a maximum values of about 4.4 at ΔP = 1.1 MPa. It is suggested that this value

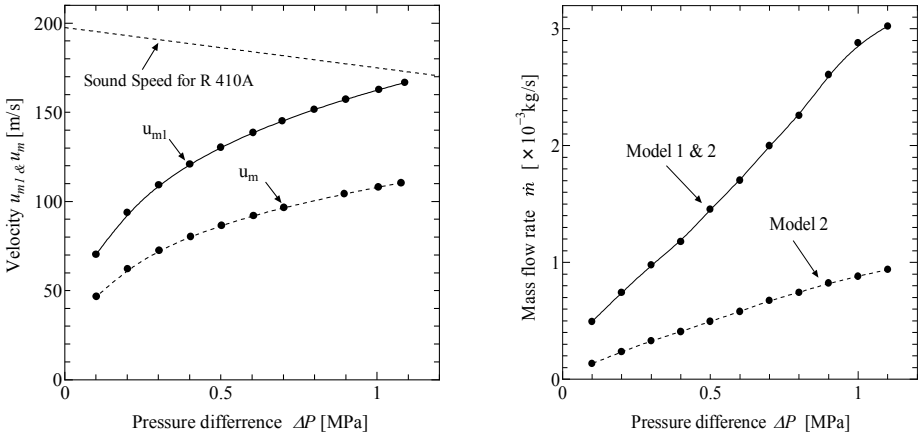

(a) Leakage flow velocities, u_{m1} and u_m. (b) Mass flow rate, $\dot{m}$.

Figure 10: Empirical data of leakage flow velocities u_{m1}, u_m, and mass flow rate $\dot{m}$ for the range of pressure differences, ΔP, considered in this study

changes depending upon the scroll curvature radius. Further detailed experiments are needed for standard scroll designs. Careful examination of the physical meaning of these values will be also needed.

5. LEAKAGE VELOCITY AND MASS FLOW RATE

In the process of the pressure decay simulations, the leakage flow velocity u_{m1} for *Model-1* and u_m for *Model-2*, and corresponding mass flow rates $\dot{m}$ have been calculated from the measured pressure drops, as shown in Figure 10(a) and 10(b), for the range of pressure differences ΔP. The leakage flow velocity u_{m1} is larger than u_m, since the passage drag is smaller for *Model-1* than for *Model-2*. However, the leakage velocity is lower than the speed of sound for R410A (shown by the dashed lines), even for highest pressure difference. It is natural that the leakage flow velocity decreases with decreasing the pressure difference ΔP.

All data of the mass flow rate $\dot{m}$ align well along the solid and dashed lines, respectively, as shown in Figure 10(b). The upper solid line is for the leakage by *Model-1&2*, and the lower dashed line is for *Model-2*, both of which increase approximately linearly with increasing the pressure difference. When the pressure difference is 1.1 MPa at maximum, the mass flow rate reaches the maximum of 3×10^{-3} kg/s for *Model-1&2* and 0.9×10^{-3} kg/s for *Model-2*. The leakage by Model-1 is far dominant. From this result, the ratio of leakage flow rates for *Model-1* to *Model-2* is about 2 to 1 for the present test set-up model.

6. CONCLUSIONS

In the present study, the hypothesized treatment of complicated bypass leakage in scroll compressors using a very simple flow model was validated. In the flow model parallel rectangular cross-section passages, classified into *Model-1* with the effective mean passage width for the radial leakage along the tip seal and *Model-2* with the effective mean passage length for the tangential leakage over the scroll wrap in front of the tip seal are used to simulate the bypass leakage flow. The effective mean passage width and the effective mean passage length were determined by very simple and easily conducted pressure decay tests, where the measured pressure decays were all successfully simulated by very simple theoretical calculations, based on the Darcy-Weisbach equation for incompressible viscous fluid flow. Furthermore, the level of contribution to the resultant leakage is examined to conclude that the leakage by *Model-1* is by far the dominant effect and the complicated bypass leakage can be calculated by just one rectangular cross-section passage represented by *Model-1*, if an error of about 5% is permissible. Finally, the effective mean passage width for *Model-1* was normalized with the representative tangential length from the contact point of the outer and inner scrolls, where the distance between the outer and inner scrolls becomes equal to the thickness of outer scroll wrap in front of

the tip seal. In this way, the reduced effective mean passage width was formulated, and the present scheme for empirically calculating the complicated bypass leakage was generalized for possible application to all cases of scroll contact area geometry.

The present study was motivated through possible developments of super large scroll compressors with shaft power more than 1000 kW, where the bypass leakage effect on the volumetric efficiency was one unknown factor for the authors. The present scheme for evaluating the complicated bypass leakage will be applied to predict the possible high volumetric efficiency of super large scroll compressors.

NOMENCLATURE

G, G_0	: Refrigerant mass	[kg]	Re	: Reynolds number	[-]
g	: Acc. of Gravity	[m/s^2]	t	: Time	[s]
L_1, L_2	: Length	[m]	$u_{m1}, u_{m2}, u_{m3}, u_{m4}$	: Mean velocity	[m/s]
l_1, l_2	: Equivalent length	[m]	W_s	: Width	[m]
$\dot{m}$	: Mass flow rate	[kg/s]	δ_a, δ_{rt}, δ_{a0}, δ_{r0}	: Clearance	[m]
n	: Polytropic index	[-]	λ	: Friction factor	[-]
$P_H, P_s, P_L, P_{12}, P_{45}$	: Pressure	[Pa]	ρ	: Density	[kg/m^3]

REFERENCES

Ishii, N., Bird, K., Sano, K., Oono, M. Iwamura, S. & Otokura, T., 1996, Refrigerant Leakage Flow Evaluation for Scroll Compressors, *International Compressor Engineering Conference at Purdue*, pp.633-638.

Ishii, N., Tsuji, T., Oku, T., Anami, K. Matsui, A. & Knisely, C., 2011, Exploration of Optimal Efficiency Super-Large Cooling Capacity Scroll Compressors for Air Conditioners, *International Conference of ICR at Prague*, ID.: 945.

Oku, T., Anami, K., Ishii, N., Knisely, C., Yasuda, K., Sawai, K. Sano, K. & Morimoto, T., 2005, Gas Leakage in CO2 and R22 Scroll Compressors and Its Use in Simulations of Optimal Performance, *International Compressor Engineering Conference at Purdue*.

Youn, Y., Cho, N., Lee, B. & Man, M., 2000, The Characteristics of Tip Leakage in Scroll Compressors for Air-Conditioners, *International Compressor Engineering Conference at Purdue*, p. 797.

NIST, 2007, Thermodynamics and Transport Properties of Refrigerants and Refrigeration Mixtures −REFPROP Version 8.0, National Institute of Standards and Techno1ogy, Gaithersburg, MD, USA.

ACKNOWLEDGEMENT

This study was initiated through research collaborations with Danfoss Commercial Compressors. The authors express their sincere gratitude the Danfoss personnel for their kind consideration. The authors extend their sincere gratitude to Mr. Takashi Morimoto, Manager, Air-Conditioning and Cold Chain Development Center, Corporate Engineering Division, and Mr. Akio Kozaki, Director, Refrigeration and Air-Conditioning Devices Business Division, Appliances Company, Panasonic Co., Ltd., for their cooperation in carrying out this work and their permission to publish this study.